encit 2020

ABCM Associação Brasileira de Engenharia e Ciências Mecânicas

18th Brazilian Congress of Thermal Sciences and Engineering
November 16-20, 2020

ENC-2020-0558
THE EFFECT OF ATHEROSCLEROSIS ON CORONARY BLOOD FLOW AND WALL DEFORMATION: A CASE STUDY USING COMPUTATIONAL FLUID DYNAMICS

Matheus Vinicius de Oliveira Herrero
Wilson Wesley Wutzow
Alexandre Marconi de Souza Costa
State University of Maringá, Maringá – Paraná
e-mail: herreromatheus93@gmail.com

Abstract: *The purpose of this paper is to develop and build a numerical model to compare two idealized left main coronary arteries (LCA), one healthy and another affected by atherosclerosis, and analyze the impact of an atherosclerotic fatty plaque in the behavior of the blood and the vascular wall. Both LCA geometries were generated based in other existing models. The blood was considered a non-Newtonian fluid and the arterial walls were modelled as Neo-Hookean solids. Literature based boundary conditions were applied and a 2-way fluid-structure interaction (FSI) coupling was set up for the two simulations. Numerical results for the velocity, pressure and wall shear stress were obtained for the fluid volume. The equivalent stresses and deformations on the wall were evaluated. The stenosis increased the peak values for all the quantities of interest analyzed. Increasing concentrations of stresses can be related to higher risks of plaque rupture. Although simplified boundary conditions were used, the results found are in accordance with other works in this field of study.*

Keywords: Numerical Methods; Atherosclerosis; Hemodynamics; Non-Linear Elasticity; Fluid-Structure Interaction.

1. INTRODUCTION

Atherosclerosis is the main cardiovascular pathology associated with aging, since its incidence grows exponentially in individuals above 45 years old (World Health Organization, 2016). An atherosclerotic lesion blocks and reduces the blood flow, causing the thickening of the vascular wall and altering its mechanical properties. The difficulty in performing in vivo experiments encourages the use of computational fluid dynamic (CFD) tools in this field. According to Karimi et al (2013), these applications include the design of prosthetics and predictive models.

Simplified geometries are frequently used to analyze intracoronary flows (Cheema and Park, 2013; Kallekar et al, 2013; Karimi et al, 2013; Cilla et al, 2015; Gholipour et al, 2018). The work done by Silveira (2017) compared patient specific geometries with simplified ones generated in CAD software and confirmed that the simplified geometries can be used to validate physical models. Although many authors have applied experimental velocity profiles (Kock et al, 2008; Cilla et al, 2015; Gholipour et al, 2018), approximate velocity functions are often used as inlet boundary conditions (Jhunjhunwala et al, 2015; Carvalho, 2017; Amiri et al, 2019).

Hemodynamics models that neglect the fluid-structure interaction (FSI) between the blood and the arterial wall exist (Legendre, 2009; Tabacow, 2014; Silveira et al, 2017) but due to the dynamic nature of the problem the use of FSI coupling methods seems inevitable as shown by El Baroudi et al (2014), Carvalho (2017), Kallekar et al (2017) e Gholipour et al (2018). In relation to blood vessels, their mechanical behavior is primarily non-linear and anisotropic (Holzapfel and Ogden, 2010). Authors tend to use various constitutive models. Hyperelastic models such as the Neo-Hookean (Cheema and Park, 2013; Karimi et al, 2013; Kallekar et al, 2017), the Mooney-Rivlin's (Das et al, 2015; Gholipour et al, 2018) and the Ogden's models (Haddad and Samani, 2017) are commonly chosen.

The importance of this field of research can be justified not just for the pursuit of better comprehension of the formation and progression of cardiovascular pathologies, but also to help in the development of better surgical methods and treatments (Bachmann et al, 2000; Yamane et al, 2004; Bessa, 2008; Legendre et al, 2008; Chabi et al, 2015). That said, the purpose of this paper is to build a numerical model in the ANSYS software to compare two idealized left main coronary arteries (LCA), one healthy and another affected by atherosclerosis, and analyze the impact of the presence of a fatty plaque in the behavior of the blood and the vascular wall.

2. THE CORONARY ARTERY MODELS

Both LCA models were built in separate stages. First, the geometries of the two LCA were defined and generated. Then, the material behavior data was inserted, and the boundary conditions were applied. Lastly, the FSI coupling was set up for the two simulations.

2.1 Geometry and Mechanical Properties

The two LCA used in the present work were based on the model created by Gholipour et al (2018) who modified the original geometry of Chen (2016) using clinical data from Holzapfel et al (2005). The generated vessel geometries had and external diameter of 4.5 mm, with a wall thickness of 0,88 mm and length equal to 16 mm with an assumed taper of 1º (Chakravarty and Mandal, 2000). For the atherosclerotic LCA in Fig. 1, a plaque with 1.26 mm height was added to create a 45% stenosis, the severity when most cases of plaque rupture occur (Sorof, 2004).

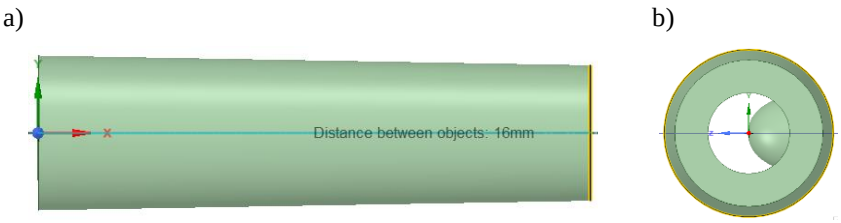

Figure 1. Geometry of the left main coronary artery: a) side view b) front view.

Although there are studies considering arterial walls as linear elastic, it is known that their behavior is primarily non-linear and anisotropic (Gundiah et al, 2009; Holzapfel and Ogden, 2010; Cheema and Park, 2013; Kallekar et al, 2017). Thus, the coronary wall was modeled as a Neo-Hookean solid. According to Boulanger (2001), the Neo-Hookean model is a hyperelastic material model that can be used to predict the stress-strain behavior of materials in a similar way to Hooke's Law. Kim et al (2012) showed how the stress-strain relation for this type of material is not linear. This hyperelastic model is widely accepted to describe the non-linear mechanical behavior in arteries (Bustamante and Holzapfel, 2010; Auricchio et al, 2011; Speelman et al, 2011).

According to Hoss (2009), the stress and strain results can be calculated through the strain energy potential function shown in Eq. 1.

$$W = \frac{G}{2}(\bar{I} - 3) + \frac{k}{2}(J - 1)^2 \tag{1}$$

In which G is the initial shear modulus, $\bar{I}$ is the first invariant of the Cauchy-Green strain tensor, k is the bulk modulus and J is the ratio between the deformed elastic volume and the undeformed volume of the solid. The bulk modulus k can be found from the incompressibility parameter d (Eq. 2).

$$k = \frac{2}{d} \tag{2}$$

The values for the initial shear modulus and the incompressibility parameter of the vascular wall were based on the experimental results of Karimi et al (2013) and were set to G=1178 MPa and d=0.045 MPa^{-1}. The specific mass of arterial wall was set to 1000 kg/m^3 (Chan et al, 2007; Gholipour et al, 2018).

2.2 Blood Flow Characteristics

As the blood flow has a cyclic and pulsatile nature, the inflow velocity was not considered constant. A waveform velocity profile based on the work by Sinnott et al (2006) was used (Eq. 3). As shown in Eq. 3, this profile has a sinusoidal shape, reaching a maximum velocity of 0.5 m/s and a minimum velocity of 0,1 m/s. A heart rate of 120 beats per minute was assumed so the duration of each cycle would be 0.5 s. The same velocity profile was used by Jhunjhunwala et al (2015), Carvalho (2017) e Amiri et al (2019).

$$v_{entrada}(t) = \begin{cases} 0.5sen[4\pi(t + 0.0160236)] : 0.5n < t \leq 0.5n + 0.218 \\ 0.1 : 0.5n + 0.218 < t \leq 0.5(n + 1) \end{cases} \tag{3}$$

At the outlet, a zero-pressure boundary condition was applied. Even though they are not realistic, constant, or zero-pressure outlet conditions are frequently used in hemodynamic studies (Boutsianis et al., 2004; Cheng et al, 2014; Osswald et al, 2017; Shang et al, 2015). This simplification often occurs because patient specific pressure profiles cannot be obtained in noninvasive ways (Shao, 2019).

As stated by Chandran et al (2007), turbulent flows can generate excessive loads on the heart or created risks to the blood cells, therefore, in this paper the blood flow was considered laminar. Other studies that considered this assumption were done by Long et al (2001), Boutsianis et al. (2004), Su et al (2014) and Wu et al. (2015). In the case of coronaries, Mahalingam et al (2016) tested turbulence models for different levels of stenosis and concluded that the flow starts to transition from laminar to turbulent when the area obstructed by the plaque exceeds 50% of the cross section. Because the blood shows pseudoplasticity, in other words, it becomes less viscous with higher shear rates, the use of a non-Newtonian fluid model seemed appropriate. The Carreau model, which can be expressed by Eq. 4, was chosen.

$$\mu_{eff} = \mu_{\infty} + (\mu_0 - \mu_{\infty})[1 + (\lambda\dot{\gamma})^2]^{\frac{n-1}{2}} \tag{4}$$

Where μ_{eff} is the effective viscosity, μ_0 is the zero-shear rate viscosity, μ_{∞} is the infinite shear rate viscosity, λ is the time constant and n is the Power Law index. The material coefficients for the blood were taken from Siebert and Fodor (2009) and are presented in Table 1.

Table 1. Input values for blood Carreau coefficients.

Carreau Coefficients	Input Values
μ_0	0.056 kg/m.s
μ_{∞}	0.0035 kg/m.s
λ	3.313 s
n	0.3568

A mesh independency study using only the fluid volume in the stenosed LCA was conducted to assure the density of elements used in its discretization was appropriate. This was made through a parametric study were the force on the fluid wall was compared for meshes of decreasing element sizes. Because blood flow is a transient problem, the convergence criteria for the residuals was set to 10^{-6} the solution was divided in 1600 time-steps of 0.0025 s. A maximum number of 5 interactions per time-step was set. A summary of this study, with the percentual difference between force results, is shown in Table 2. Only tetrahedral linear elements were used in the generated meshes.

Table 2. Mesh independence study.

Element Size (mm)	Number of Nodes	Number of Elements	Wall Force (N)	Difference (%)
0.8	383	1326	0.0003579	-
0.4	2324	10457	0.0004067	13.61%
0.2	15661	80930	0.0004317	6.15%
0.1	114713	635944	0.0004411	2.18%

Using the independence studies of Boutsianis et al (2004) and Mahalingam et al (2016), a criterion of 5% maximum difference between force values was adopted. As the wall force differed only 2.18% when the element number increase from 80930 to 635944, the mesh with element size of 0.2 mm was assumed to have reached independence. The mesh for the fluid volume is shown in Fig. 2 a).

a) b)

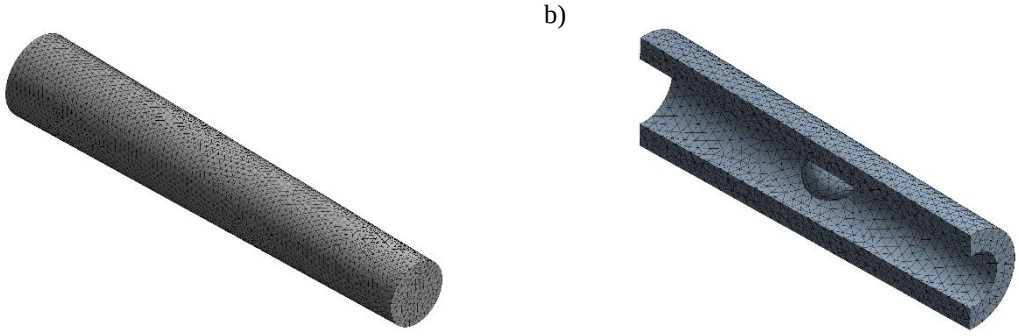

Figure 2. Converged meshes for stenosed LCA: a) Fluid volume LCA b) Solid volume.

2.3 Fluid-Structure Interaction Coupling

The FSI coupling was made through System Coupling tool in Ansys Workbench. Meshes of tetrahedral quadratic elements were generated for both coronary models. The element size chosen for the solid mesh was 0,4 mm as shown in Fig. 2 b). A coarser solid mesh is preferable when using System Coupling because of the algorithms used to transfer the force and displacement results between the CFD and the finite element analysis (FEA) models. A 2-way FSI was set up, where the results of force and displacement were transferred between the fluid and solid volumes at each FSI coupling interaction. According to Carvalho (2017), although the 2-way coupling is computationally expensive, its advantage lies in the greater reliability of the results it can provide.

A time-step of 0.0025 s was chosen and a maximum number of 5 coupling interactions per time-step was defined. The flow was given an end-time of 4.0 s to assure the solution would be converged when the last cycle of the velocity profile was reached (between 3.5 and 4.0 s). Also, to better model the displacement of the fluid-solid interface, a Dynamic Mesh tool, with Smoothing and Remeshing options was added to the fluid wall. The two LCA were fixed at the extremities using a no-displacement condition. After all the coupling interactions were finished, it was observed that the convergence criteria of 10^{-6} for the residuals was met for both the solid and fluid volumes. The contour plots for the converged simulations were then extracted and analyzed.

3. RESULTS AND DISCUSSIONS

The results focused in capturing contour plots and comparison curves to observe the changes in the flow behavior in the presence of the plaque and to analyze the main factors of influence to plaque rupture in the stenosed LCA.

3.1 Numerical Results: Fluid Volume

Figure 3 show the average velocities through the 4 s of blood flow in the central plane for the fluid volume. In Fig. 2 b), the disturbance caused to the flow by the stenosis is clear. In the same way as shown by Cilla et al (2015), Kallekar et al (2017) e Gholipour et al (2018), the region of higher velocities was located close to the plaque. The value for maximum velocity found for the stenosed LCA was 10.51% higher than that of the healthy one. In both cases, the velocities were zero close to the wall due to the no-slip condition.

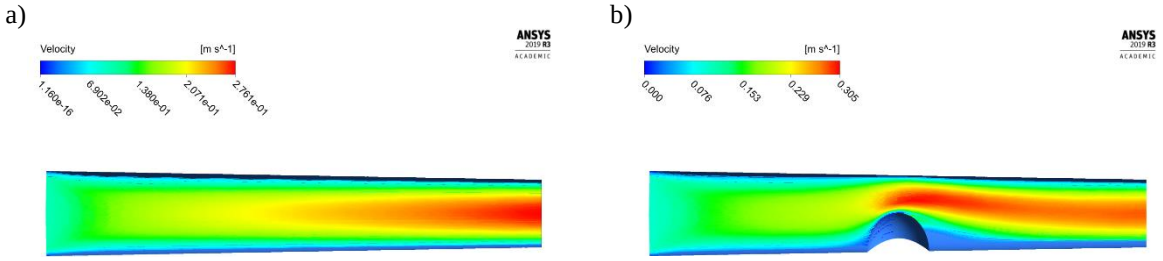

Figure 3. Velocity distribution for the blood on the central plane: a) No stenosis LCA b) 45% stenosis LCA.

As visible in Fig.4, the pressure contours on the blood-wall interface show a more uniform distribution throughout the geometry of the healthy LCA, while for the model with 45% stenosis the pressure drop was more abrupt. The presence of the plaque creates a narrower band of intermediary values. The maximum pressure result for the stenosed vessel was 22.77% higher. Although the plaque has shown the same general pressure distribution, the absolute values found by Gholipour et al (2018) for an LCA with 45% stenosis are 10 times higher than the ones in this paper. The difference is significant but justifiable due to the assumption of the zero-pressure boundary condition for the outlet, which would clearly decrease the average pressure values in the volume of blood that was modelled.

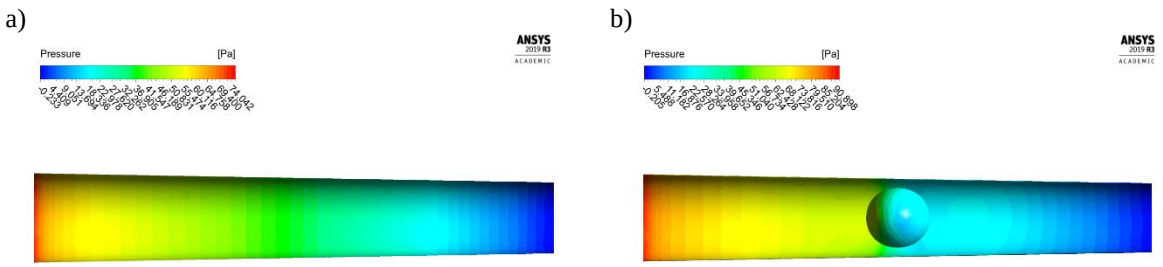

Figure 4. Pressure distribution for the blood: a) No stenosis LCA b) 45% stenosis LCA.

The wall shear stress results shown in Fig. 5 follow the pressure patterns, where the distribution varies more quickly on the obstructed region. The cap of the plaque suffered the highest amount of shear stress and the maximum result for the atherosclerotic LCA was 36.90% higher than for the healthy one.

Comparing these results with other works where simplified blood vessel geometries were used, Mahalingam et al (2016) also used zero-pressure outlet condition and achieved wall shear stresses only 13.68% higher than the ones found in this paper. On the other hand, for studies where transient pressure profiles were used as boundary condition for the outflow of the artery (Cilla et al, 2015 and Gholipour et al, 2018) the results reached higher values (up to 110% difference).

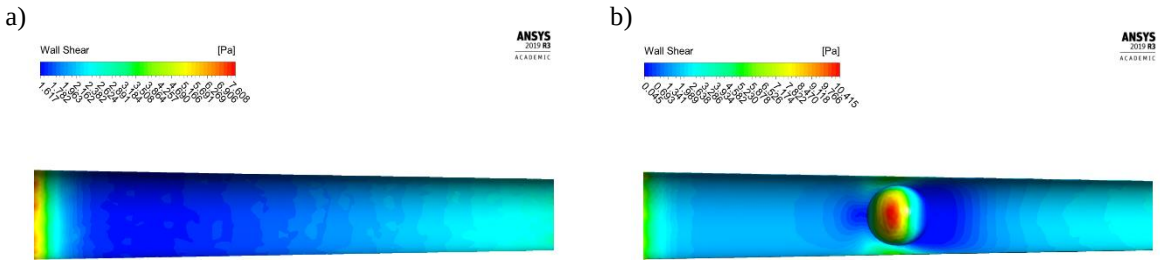

Figure 5. Wall shear stress for the blood: a) No stenosis LCA b) 45% stenosis LCA.

Table 3 summarizes the comparisons made between the maximum and minimum total equivalent stress results found for each LCA model along their percentual differences.

Table 3. Difference between results found for the fluid volumes of both LCA models.

		No Stenosis	45% Stenosis	Difference (%)
Velocity (m/s)	Max.	0.276	0.305	10.51%
	Min.	0	0	-
Pressure (Pa)	Max.	74.040	90.898	22.77%
	Min.	-0.233	-0.205	-12.09%
Wall Shear Stress (Pa)	Max.	7.608	10.415	36.90%
	Min.	1.617	0.0450	-97.22%

3.2 Numerical Results: Solid Volume

The equivalent Von Misses stresses and the deformation of the coronary wall were computed. The contour plots for the times 3.6 and 3.8 are presented in Fig. 6, as well as the curves for their values during the last cycle of the velocity profile (from 3.5 to 4.0 s). In the non-stenosed artery, although there was an increase in the value of the stresses found, their distribution along the remained the same. The maximum total stresses concentrated on the region close to the inlet of LCA. For the case where the plaque was present, two new regions of low stress were visualized, one on the cap of the plaque and another small area downstream of the plaque. Additionally, an asymmetric strip of intermediary stresses was located at upstream side of the base of the plaque.

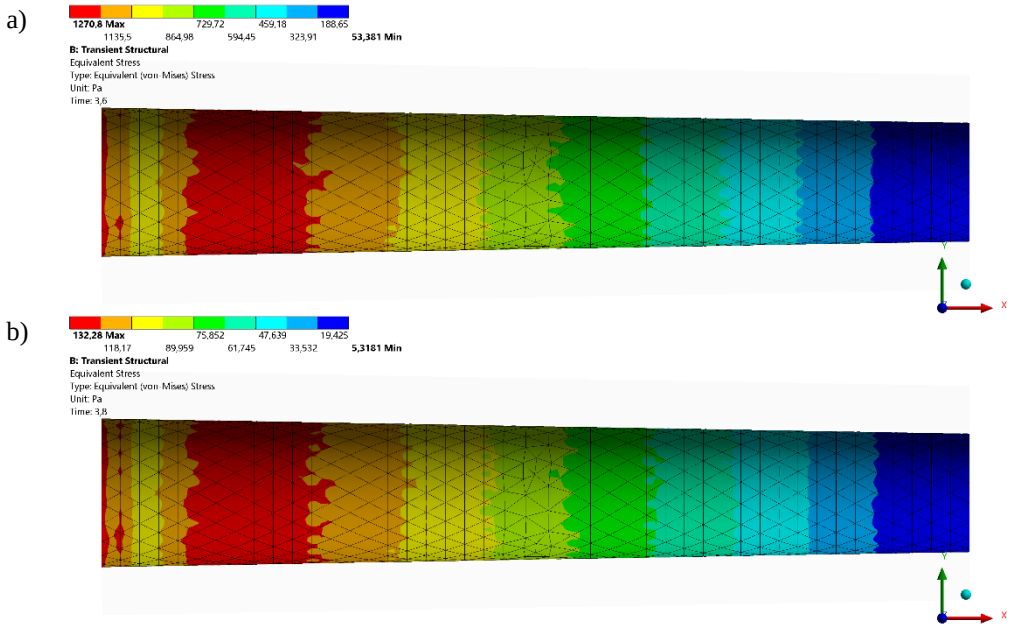

Figure 6. Equivalent Von Mises stress on the LCA wall with no stenosis: a) At 3.6 s b) At 3.8 s.

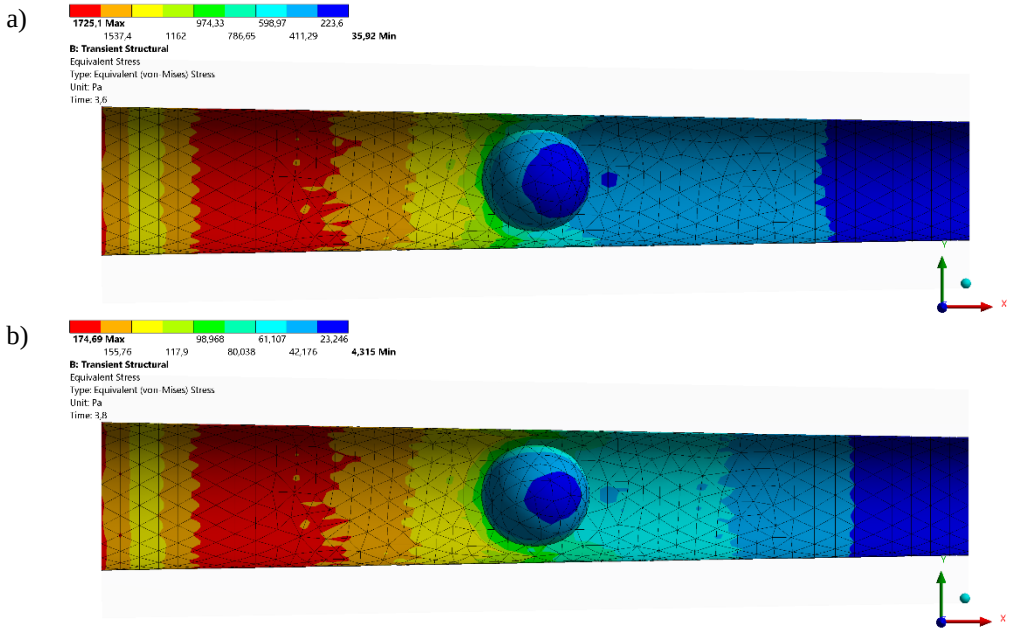

Figure 7. Equivalent Von Mises stress on the LCA wall with 45% stenosis: a) At 3.6 s b) At 3.8 s.

When the maximum equivalent stresses for both models were compared, an increase of 35.75% was found in the model with 45% stenosis. A curve showing their change in maximum equivalent stresses during a heartbeat is shown in Fig. 10 a). The areas where the wall suffered more deformation (Fig. 8) overlap with those of maximum equivalent stress. The appearance of zero-deformation areas on both extremities of the LCA were expected due to the boundary conditions applied to fix que coronary on que mechanical analysis. On the partially obstructed geometry (Fig. 9), the minimum deformation region extended from the outlet up to the root of the plaque. Differences of 38,0% were calculated between the total maximum deformation results for both LCA models. A curve showing the change in maximum total deformation for both cases during a heartbeat is shown in Fig. 10 b).

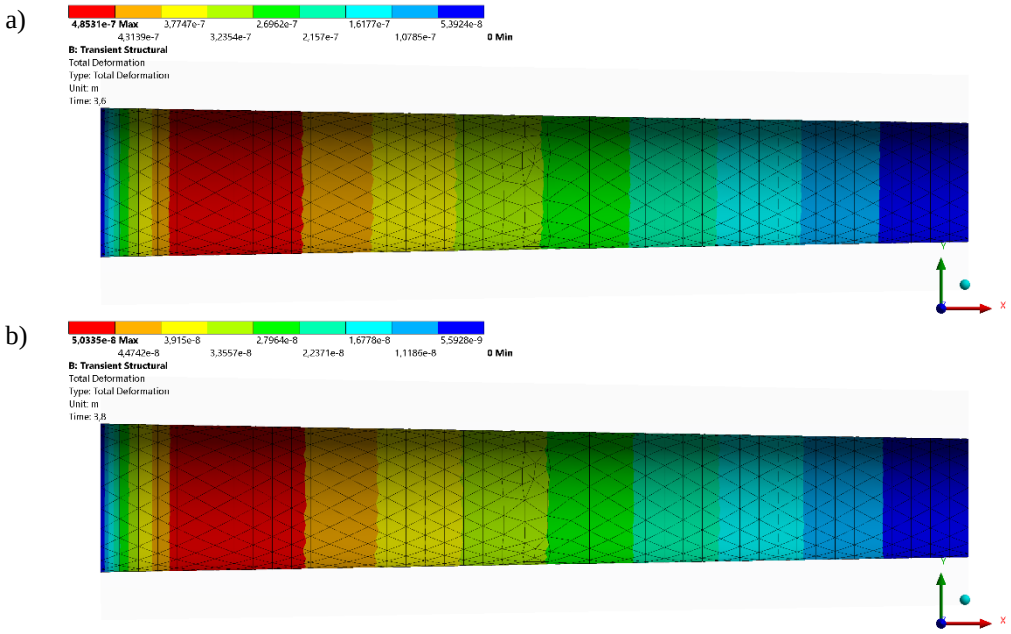

Figure 8. Total deformation on the LCA wall with no stenosis: a) At 3.6 s b) At 3.8 s.

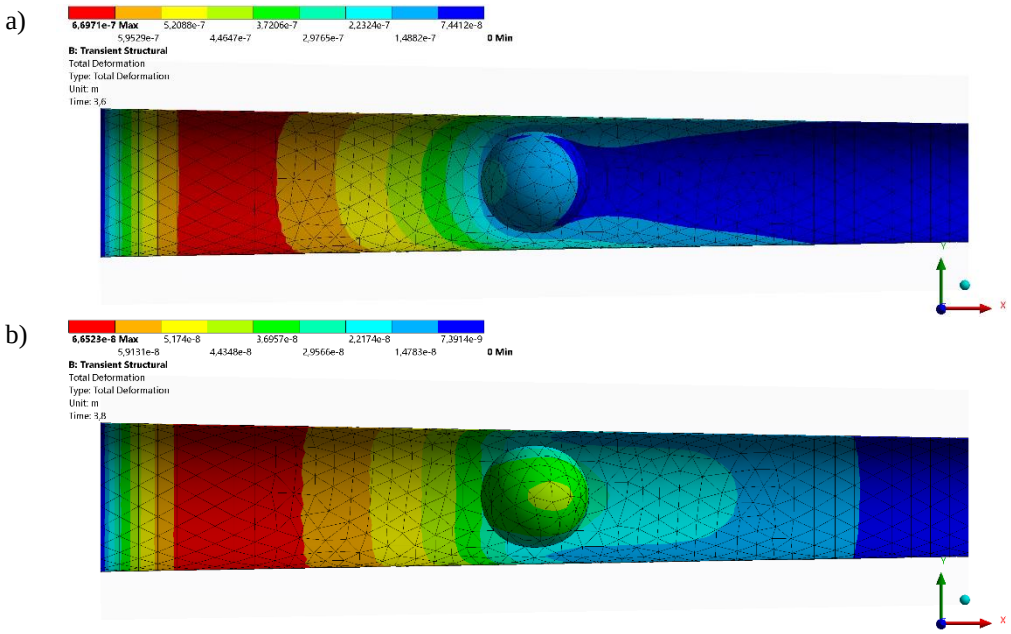

Figure 9. Total deformation on the LCA wall with 45% stenosis: a) At 3.6 s b) At 3.8 s.

Consulting other studies about stenotic blood vessels, it is possible to see a clear relation between the magnitudes of flow velocity and the dimension of the wall deformations. While Kallekar et al (2017) found deformations around 2 mm for a peak velocity of 2 m/s, Cheema and Park (2013) applied a normal velocity of 100 μm/s and visualized lower values of deformation. Both these works considered the vascular wall as a Neo-Hookean material. Lastly, the Cheema and Park (2013) model would only attain close to 45% the maximum deformation found in the present paper for a case of a blood vessel with more than 90% stenosis severity.

a)

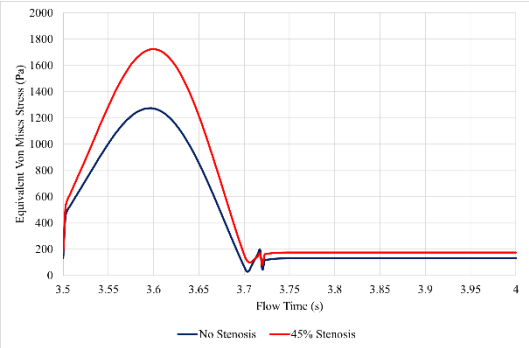

b)

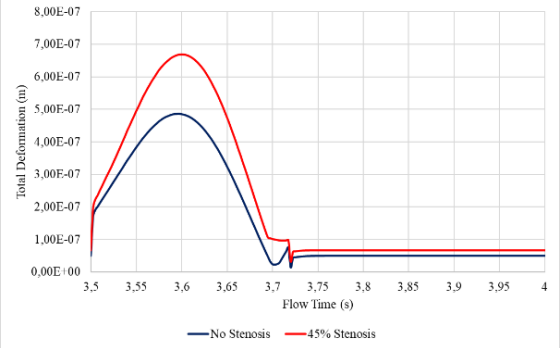

Figure 10. Comparison of results for both LCA models: a) Equivalent Von Mises Stress b) Total Deformation.

Table 4 summarizes the comparisons made between the maximum and minimum total deformation results found for each LCA model along their percentual differences.

Table 4. Difference between results found for the solid volumes of both LCA models.

		No Stenosis	45% Stenosis	Difference (%)
Equivalent Von Mises Stress (Pa)	Max.	1270.80	1725.10	35.75%
	Min.	132.28	174.69	32.06%
Total Deformation (m)	Max.	4.85E-07	6.70E-07	38.00%
	Min.	5.03E-08	6.65E-08	32.16%

4. CONCLUSIONS

In this paper, a numerical model of a left main coronary artery was developed to evaluate the effects of atherosclerosis on the characteristics of blood flow and wall behavior in comparison with a healthy artery. In order to represent the phenomenon of blood flow more accurately, the following assumptions were adopted in the model: pulsatile flow, non-Newtonian viscosity for the blood and 2-way fluid-structure interaction with hyperelastic constitutive model for the vascular wall. Idealized geometries were used for both LCA and simplified zero-pressure outlet conditions were applied. The numeric results were analyzed in two sections referring to the fluid and solid volume. For the fluid (blood) volume, the velocity, pressure and wall shear stress were evaluated, while for the solid (arterial wall) volume, the equivalent Von Mises Stresses and the total deformations were computed for a cardiac cycle of 0.5 s.

An increase in the maximum values of velocity (10.51%), pressure (22.77%) and wall shear stress (36.90%) was observed when the atherosclerotic plaque was introduced in the model and, although the minimum values for velocity remained the same, a decrease in the minimum values for pressure (-12.09%) and wall shear stress (-97.22%) also occurred. When the equivalent Von Mises stresses for both models were compared, the values for the 45% stenosed LCA were 35.75% higher during peak systole and 32.06% higher during diastole. The total deformations found had similar percentual differences, being 38.00% higher during peak systole and 32.16% higher during diastole for the model where stenosis was considered.

The presence of atherosclerotic plaque caused the elevation of the peak values for all the quantities of interest analyzed. Increasing concentrations of stresses can be related to higher risks of plaque rupture. The 2-way fluid-structure coupling proved to be an important tool in creating a model that better mirrored the interaction between blood flow and arterial wall seen in experimental results. Although simplified boundary conditions were made, the behavior of both volumes and the distribution of the quantities evaluated were found to be in accordance with other works in this field of study.

5. REFERENCES

Amiri, Mohammad Hassan, et al. "A 3-D numerical simulation of non-Newtonian blood flow through femoral artery bifurcation with a moderate arteriosclerosis: investigating Newtonian/non-Newtonian flow and its effects on elastic vessel walls." *Heat and Mass Transfer* 55.7 (2019): 2037-2047.

Auricchio, Ferdinando, et al. "Carotid artery stenting simulation: from patient-specific images to finite element analysis." *Medical engineering & physics* 33.3 (2011): 281-289.

Bachmann, Christopher, et al. "Fluid dynamics of a pediatric ventricular assist device." *Artificial Organs* 24.5 (2000): 362-372.

Bessa, Kleiber Lima de. *Redução de arrasto por adição de polímeros em escoamento pulsátil laminar e turbulento em leitos arteriais caudais de ratos normotensos e hipertensos e tubos rígidos*. Diss. Universidade de São Paulo, 2008.

Boutsianis, Evangelos, et al. "Computational simulation of intracoronary flow based on real coronary geometry." *European journal of Cardio-thoracic Surgery* 26.2 (2004): 248-256.

Bustamante, R., and Gerhard A. Holzapfel. "Methods to compute 3D residual stress distributions in hyperelastic tubes with application to arterial walls." *International Journal of Engineering Science* 48.11 (2010): 1066-1082.

Carvalho, Jeane Batista de. "Estudo numérico hemodinâmico de um aneurisma na vizinhança de uma bifurcação arterial tridimensional." (2017).

Chabi, Fatiha, et al. "Critical evaluation of three hemodynamic models for the numerical simulation of intra-stent flows." *Journal of biomechanics* 48.10 (2015): 1769-1776.

Chakravarty, Santabrata, and Prashanta Kumar Mandal. "Two-dimensional blood flow through tapered arteries under stenotic conditions." *International Journal of Non-Linear Mechanics* 35.5 (2000): 779-793.

Cheema, Taqi Ahmad, and Cheol Woo Park. "Numerical investigation of hyperelastic wall deformation characteristics in a micro-scale stenotic blood vessel." *Korea-Australia Rheology Journal* 25.3 (2013): 121-127.

Chen, Colin Xu. "Modelling of atherosclerotic plaque growth using fluid–structure interaction." *Bulletin of the Australian Mathematical Society* 93.1 (2016): 170-172.

Cheng, Z., et al. "Predicting flow in aortic dissection: comparison of computational model with PC-MRI velocity measurements." *Medical engineering & physics* 36.9 (2014): 1176-1184.

Cilla, M., et al. "A parametric model for analysing atherosclerotic arteries: On the FSI coupling." *International Communications in Heat and Mass Transfer* 67 (2015): 29-38.

Das, Ashish, et al. "Pulsatile arterial wall-blood flow interaction with wall pre-stress computed using an inverse algorithm." *Biomedical engineering online* 14.S1 (2015): S18.

El Baroudi, Adil, Fulgence Razafimahéry, and Lalaonirina Rakotomanana. "Fluid–structure interaction within three-dimensional models of an idealized arterial wall." *International Journal of Engineering Science* 84 (2014): 113-126.

Gholipour, Alireza, et al. "Three-dimensional biomechanics of coronary arteries." *International Journal of Engineering Science* 130 (2018): 93-114.

Gundiah, Namrata, Mark B. Ratcliffe, and Lisa A. Pruitt. "The biomechanics of arterial elastin." *Journal of the Mechanical Behavior of Biomedical Materials* 2.3 (2009): 288-296.

Haddad, Seyyed MH, and Abbas Samani. "A computational model of the left ventricle biomechanics using a composite material approach." *International Journal of Engineering Science* 111 (2017): 61-73.

Holzapfel, Gerhard A., et al. "Determination of layer-specific mechanical properties of human coronary arteries with nonatherosclerotic intimal thickening and related constitutive modeling." *American Journal of Physiology-Heart and Circulatory Physiology* 289.5 (2005): H2048-H2058.

Holzapfel, Gerhard A., and Ray W. Ogden. "Constitutive modelling of arteries." *Proceedings of the Royal Society A: Mathematical, Physical and Engineering Sciences* 466.2118 (2010): 1551-1597.

Hoss, Leonardo. "Modelos constitutivos hiperelásticos para elastômeros incompressíveis: ajuste, comparação de desempenho e proposta de um novo modelo." (2009).

Jhunjhunwala, P., P. Padole, and S. Thombre. "CFD Analysis of Pulsatile Flow and Non-Newtonian Behavior of Blood in Arteries." *Mol Cell Biomech* 12.1 (2015): 37-47.

Kallekar, Laxman, Chinthapenta Viswanath, and Mohan Anand. "Effect of wall flexibility on the deformation during flow in a stenosed coronary artery." *Fluids* 2.2 (2017): 16.

Karimi, Alireza, et al. "A finite element investigation on plaque vulnerability in realistic healthy and atherosclerotic human coronary arteries." *Proceedings of the Institution of Mechanical Engineers, Part H: Journal of Engineering in Medicine* 227.2 (2013): 148-161.

Kim, Beomkeun, et al. "A comparison among Neo-Hookean model, Mooney-Rivlin model, and Ogden model for chloroprene rubber." *International Journal of Precision Engineering and Manufacturing* 13.5 (2012): 759-764.

Legendre, Daniel, et al. "Computational fluid dynamics investigation of a centrifugal blood pump." *Artificial Organs* 32.4 (2008): 342-348.

Legendre, Daniel Formariz. *Estudo de comportamento de fluxo através de modelo físico e computacional de aneurisma de aorta infra-renal obtido por tomografia*. Diss. Universidade de São Paulo, 2009.

Long, Q., et al. "Numerical investigation of physiologically realistic pulsatile flow through arterial stenosis." *Journal of Biomechanics* 34.10 (2001): 1229-1242.

Mahalingam, Arun, et al. "Numerical analysis of the effect of turbulence transition on the hemodynamic parameters in human coronary arteries." *Cardiovascular diagnosis and therapy* 6.3 (2016): 208.

Osswald, A., et al. "Elevated wall shear stress in aortic type B dissection may relate to retrograde aortic type A dissection: a computational fluid dynamics pilot study." *European Journal of Vascular and Endovascular Surgery* 54.3 (2017): 324-330.

Shang, Eric K., et al. "Use of computational fluid dynamics studies in predicting aneurysmal degeneration of acute type B aortic dissections." *Journal of vascular surgery* 62.2 (2015): 279-284.

Shao, Clementine. "Images and models for decision support in aortic dissection surgery." (2019).

Siebert, Mark W., and Petru S. Fodor. "Newtonian and non-newtonian blood flow over a backward-facing step–a case study." *Proceedings of the COMSOL Conference*. 2009.

Sinnott, Matthew, Paul W. Cleary, and Mahesh Prakash. "An investigation of pulsatile blood flow in a bifurcation artery using a grid-free method." *Proc. Fifth International Conference on CFD in the Process Industries*. 2006.

Sorof, S. "Intravascular Atheroma Monitoring: Past, Present and Future of identifying Vulnerable Plaques." *Applications in Imaging-Cardiac interventions* (2004): 34-39.

Speelman, Lambert, et al. "Initial stress in biomechanical models of atherosclerotic plaques." *Journal of biomechanics* 44.13 (2011): 2376-2382.

Su, Boyang, et al. "Numerical investigation of blood flow in three-dimensional porcine left anterior descending artery with various stenoses." *Computers in biology and medicine* 47 (2014): 130-138.

Tabacow, Fabio Bittencourt Dutra. *Análise computacional de esforços hemodinâmicos em aneurisma de aorta abdominal infra-renal antes e após a instalação de endopróteses*. Diss. Universidade de São Paulo, 2014.

World Health Organization. *World health statistics 2016: monitoring health for the SDGs sustainable development goals*. World Health Organization, 2016.

Wu, Jianhuang, et al. "Transient blood flow in elastic coronary arteries with varying degrees of stenosis and dilatations: CFD modelling and parametric study." *Computer Methods in Biomechanics and Biomedical Engineering* 18.16 (2015): 1835-1845.

Yamane, Takashi, et al. "A comparative study between flow visualization and computational fluid dynamic analysis for the Sun Medical centrifugal blood pump." *Artificial organs* 28.5 (2004): 458-466.

6. RESPONSIBILITY NOTICE

The authors are the only responsible for the printed material included in this paper.